ISSN: 2476- 2334

Research Article

International Journal of Nanotechnology & Nanomedicine

Chemical Combination of 4-(4-Hydroxybut-2-ynyl) Pyridine and 3-Methylbenzenamine to Construct an Effective Inhibitor: Theoretical and Practical Investigation

Rujang He[1], Guangqang Xia[1], Xiaohui Jiang[1]*, Yunwen Liao[1], Qiang Pu[2] and Ming Duan[3]

[1]*Chemical Synthesis and Pollution Control Key Laboratory of Sichuan Province, China West Normal University, Nanchong, Sichuan, PR China*

[2]*China Petroleum Engineering Co.,Ltd Southwest Company, Chengdu, Sichuan, PR China*

[3]*State Key Laboratory of Oil and Gas Reservoir Geology and Exploitation, Southwest Petroleum University, Chengdu, Sichuan, PR China*

***Corresponding author**

Xiaohui Jiang, 1Chemical Synthesis and Pollution Control Key Laboratory of Sichuan Province, China West Normal University, Nanchong, Sichuan, PR China, Email id: jxh2314508@163.com

Submitted: 12 Sep 2018; **Accepted**: 19 Sep 2018; **Published**: 28 Sep 2018

Abstract

A new inhibitor, N-m-benzylamine-4-(4-hydroxybut-2-ynyl) pyridinium bromide (designated as BAP) was designed and synthesized. Quantum chemical calculation and molecular dynamics (MD) simulations manifested that BAP, a compound by covalent combination of 4-(4-hydroxybut-2-ynyl) pyridine (HYP) and 3-methyl benzenamine (MBA), functioned better than did the two moieties (HYP and MBA) for X70 steel corrosion inhibition. The corrosion inhibition investigation revealed that the experiment outcome was in good consistency with the theoretical calculation. The inhibition efficiency of BAP was 95.72% for X70 steel in 5 M HCl at 90 0C. BAP adsorbed on X70 steel surface, obeyed Langmuir isotherm, retarded both the metal dissolution and the hydrogen evolution, and enhanced greatly the acid corrosion resistance of X70 steel. Comparative test demonstrated that the inhibition efficiency of BAP was about 10 times of that for MAB and 8 times of that for HYP albeit the concentration of BAP was tenth of that of HYP and MBA. The experimental investigation backs up the theoretical calculation and manifests intramolecular synergism of the structure moieties being beneficial to design of high effective inhibitors.

Keywords: Mild Steel, Weight Loss, Eis, Acid Inhibition, Quantum Chemical Calculation

Introduction

Carbon steel is one of the most commonly used constructional materials in many fields owing to its low cost, good tensile strength and availability [1, 2]. However, it is highly sensitive to corrosion, especially in acidic media [3, 4]. Acid solutions, especially hydrochloric acid, are widely used in industries for acid picking, acid cleaning, acid descaling and oil well acidizing [5]. Therefore, widespread corrosion problems are encountered in industry. Acid corrosion may not have a deleterious effect on materials immediately, but it affects the strength, mechanical operations, and physical appearance of materials in general, leading to serious operational problems and tremendous economic losses. The employment of inhibitors is one of the most effective methods for protection of metals against corrosion [6, 7]. The inhibition of organic inhibitors follows the adsorption mechanism.

The adsorbing molecule mitigates the rate of corrosion of metals in corrosive medium. The inhibition efficiency of organic inhibitors depends mainly on the chemical structure. It is well known that most of acid corrosion inhibitors contain electronegative atoms (such as, N, O, and S), the unsaturated bonds (such as double bonds or triple bonds) and the conjugated systems including all kinds of aromatic rings [10-12]. For instance, –NH2 groups in the structures of inhibitors often act as reaction centers amino during the adsorption of inhibitors. In this way, organic inhibitors form an adsorbed protective film on metal surface, and protect metals from the attack of acid solutions [13-16]. In addition, many kinds of nitrogen-containing compounds such as pyridine and its derivatives also attract attention due to their inhibition properties for metal corrosion [17, 18]. The nitrogen atom of high electron density at the pyridine ring and its electron donating power to the metal ions are likely to facilitate the adsorption action on metal surface. Furthermore, molecules containing acetylene alcohols are claimed to form a film on the metal surface and retard the metal dissolution process (an anodic reaction) as well as hydrogen evolution (a cathodic reaction). So, propargyl alcohol is widely used to mitigate the corrosion of metals in acid media in high temperature [19, 20].

In the present work, we attempt to construct a molecule containing amino, pyridine, propargyl alcohol and benzene ring, hoping that this molecule has better anticorrosion performance. Therefore, N-m-benzylamine-4-(4-hydroxybut-2-ynyl) pyridinium bromide is designed and synthesized. The corrosion inhibition performance of BAP on X70 steel is first evaluated by quantum chemical calculation and molecular dynamic simulation, then by means of weight loss, Tafel polarization, and electrochemical impedance spectroscopy measurements of X70 steel in hydrochloric acid solution. At last,

the inhibition efficiency of BAP is compared with those of the two moieties.

Experiments

Materials and instruments: 3-(bromomethylene) phenylcarbamic acid tert-butyl ester was purchased from Shanghai Changfeng biomedical technology Co., Ltd, China. Hydrochloric acid (37%), 4-chloromethylpyridine hydrochloride (99%), and propargyl alcohol (98%) were all purchased from Chengdu Kelong Company, China. All reagents were used as supplied except propargyl alcohol which was distilled before use. Bruker-400 NMR spectrometer (Germany), Nicolet-6700 FT-IR spectrometer (USA) and waters Q-TOF Premier mass spectrometer (Germany) were employed to confirm the structure of BAP and CHI760E electrochemical workstation for electrochemical measurements.

X70 steel is donated by Petrochina Southwest Oil & Gasfield Company and the chemical composition is listed in [Table 1].

Table 1: Chemical composition of X70 steel specimen

Element	P	S	C	Si	Mn	Ti	Mo	V	Nb	Fe
Weight (%)	0.02	0.01	0.16	0.45	1.70	0.06	0.35	0.06	0.05	Balanced

Quantum chemical calculation

Quantum chemical calculation was carried out to evaluate the possibility of enhanced inhibition of BAP using the density functional theory (DFT) method involving the Becke three-parameter hybrid functional together with the Lee-Yang Paar correlation functional (B3LYP). The 6-31G(d, p) basis set was chosen for all the calculation. The calculation was carried out with the aid of Gaussian 09 software. The relevant quantum chemical parameters were calculated, such as the frontier molecular orbital energies (E_{HOMO}, E_{LUMO}), Mulliken charges, dipolar moment (μ), total energy and molecular volume (V). Other parameters such as the energy gap (ΔE), ionization potential (I), global electrophilicity index (ω), electron affinity (A), global chemical softness (S) global hardness (η), and electronegativity (x) were computed according to the following equations [21, 22], respectively.

$$I = -E_{HOMO} \quad (1)$$

$$A = -E_{LUMO} \quad (2)$$

$$\chi = \frac{I + A}{2} \quad (3)$$

$$\eta = \frac{I - A}{2} \quad (4)$$

$$S = \frac{1}{\eta} \quad (5)$$

$$\omega = \frac{\chi^2}{2\eta} \quad (6)$$

Molecular dynamic simulation

The interaction between BAP and Fe surface was investigated by MD simulation using Material Studio 7.0. The MD simulations was carried out in a simulation box (5.7138 nm × 5.7138 nm × 3.7857 nm) with periodic boundary conditions to model a representative part of the interface devoid of any arbitrary boundary effects. The (100) plane of iron substrate was optimized for minimum energy, the inhibitor molecule was placed near to the surface, and the behavior of the molecule was simulated on the Fe (100) surface by the COMAPSS force field. Three layers of iron atoms were used to ensure that the depth of the surface was greater than the non-bond cutoff radius used in the calculation. The MD simulation was performed at 298 K and controlled by the Andersen thermostat, NVT ensemble, with a time step of 1.0 fs and simulation time of 1000 ps.

The interaction energy as well as binding energy between the inhibitor molecules and Fe (100) surface was calculated using Equations. (7) and (8).

$$E_{interaction} = E_{total} - (E_{surface} + E_{inhibitor}) \quad (7)$$

$$E_{binding} = -E_{interaction} \quad (8)$$

Where E_{total} is the total energy of the surface and adsorbed inhibitor molecule, $E_{surface}$ is the energy of the surface without the inhibitor and $E_{inhibitor}$ is the energy of the adsorbed inhibitor molecule on the surface. The binding energy of the inhibitor molecule is the negative value of the interaction energy [23]. Charge effects were ignored in simulations and all calculations were performed at the metal/vacuum interface.

Synthesis of BAP

BAP is prepared by chemical combination of MBA and HYP following the steps in Figure 1 and the procedure described as follows [24].

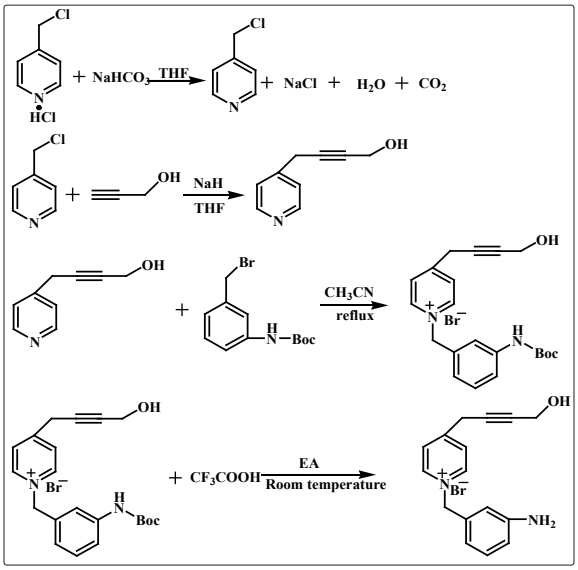

Figure 1: The preparation route of N-m-benzylamine-4-(4-hydroxybut-2-ynyl) pyridinium bromide.

4-chloromethylene pyridine hydrochloride (0.1mol), sodium bicarbonate (0.15mol) and THF (50 mL) were mingled under agitation for 6 h at 70 °C. Then, the mixture was filtered; dark black liquid was collected and dried by anhydrous $MgSO_4$ over night. After MgSO4 was removed by filtration, a dark black liquid was collected for the next reaction.

Sodium hydride (0.15mol) was suspended in THF (50 ml) and stirred under nitrogen atmosphere at room temperature. Propargyl alcohol (0.12mol) was added to the above solution and the mixture was refluxed for 4 h at 60 °C. Next, the above obtained dark black liquid was added and the mixture was continuously refluxed for 48 h. Subsequently, the mixture was filtered, the desired liquid concentrated and the liquid was further purified by column chromatography and 4-(4-hydroxybut-2-ynyl) pyridine was obtained with a yield of 92%.

4-(4-hydroxybut-2-ynyl) pyridine (0.0077 mol), and 3-bromomethylene phenylcarbamic acid tert-butyl ester (0.007 mol) were mixed thoroughly in acetonitrile (25 ml) and stirred for 72 h at 60 °C. The mixture was concentrated and purified through a silica gel column (CH_2Cl_2:CH_3OH=70:1). Then a white viscous solid was collected with a yield of 88%.

A mixture liquid of trifluoroacetic acid (3 mL), dichloromethane (3.33 mL) and BAP-Boc (2 g) was mixed and stirred at 45 °C for 12 h. After the solvent being evacuated, the saturated Na_2CO_3 solution was added to adjust the pH of the solution to 8-9. The mixture was extracted with ethyl acetate for at least three times, and the organic layer is concentrated and dried on anhydrous $MgSO_4$ over night. $MgSO_4$ and ethyl acetate was removed and the residue passed through a silica gel column (CH_2Cl_2 / CH_3OH = 30/1). Then, N-m-benzylamine-4-(4-hydroxybut-2-ynyl) pyridinium bromide, a pale yellow, viscous solid, was obtained with a yield of 93%. The structure of the intermediates and BAP were confirmed by NMR and FT-IR (Supplementary Materials Figures.S1–S11).

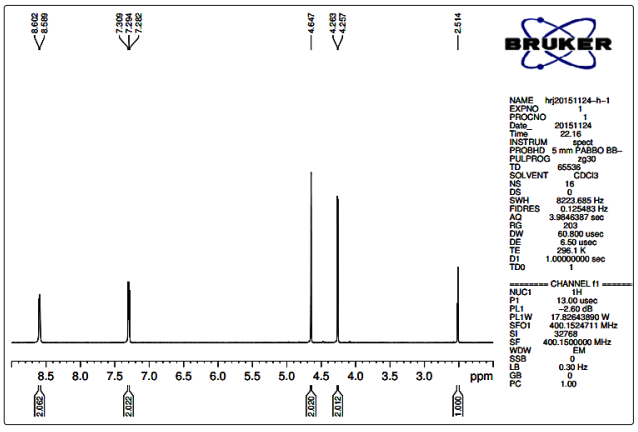

Figure S1: The 1H NMR of 4-(pyridin-4-yl)but-2-yn-1-ol

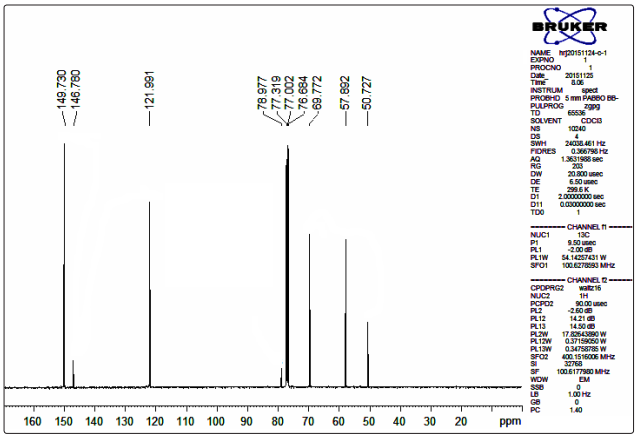

Figure S2: The 13C NMR of 4-(pyridin-4-yl)but-2-yn-1-ol

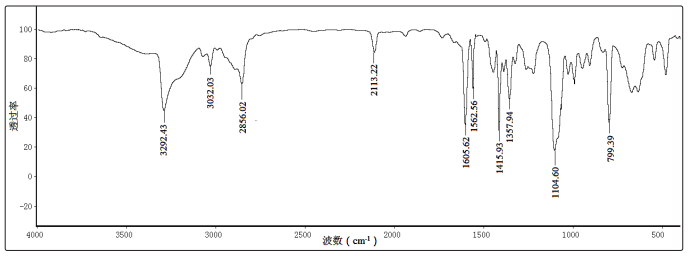

Figure S3: The FT-IR spectrum of 4-(pyridin-4-yl)but-2-yn-1-ol

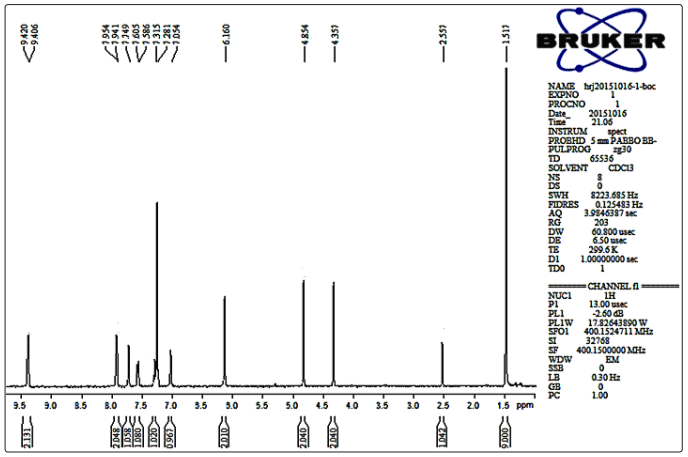

Figure S4: The 1H NMR of BAP-Boc

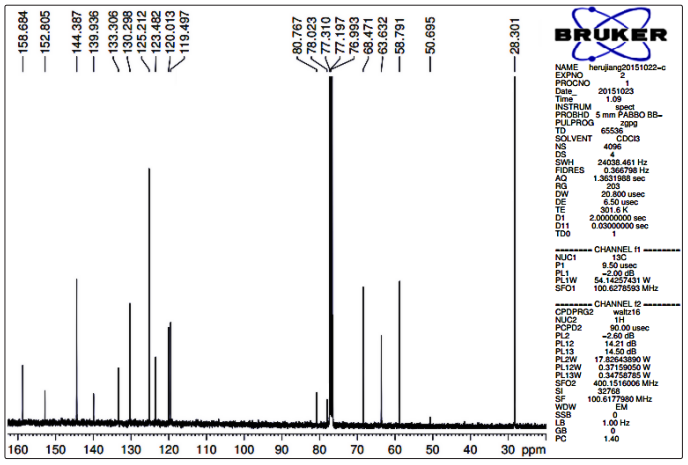

Figure S5: The 13C NMR of BAP-Boc.

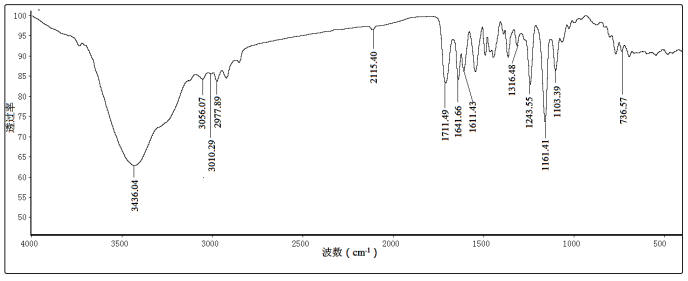

Figure S6: The FT-IR spectrum of BAP-Boc

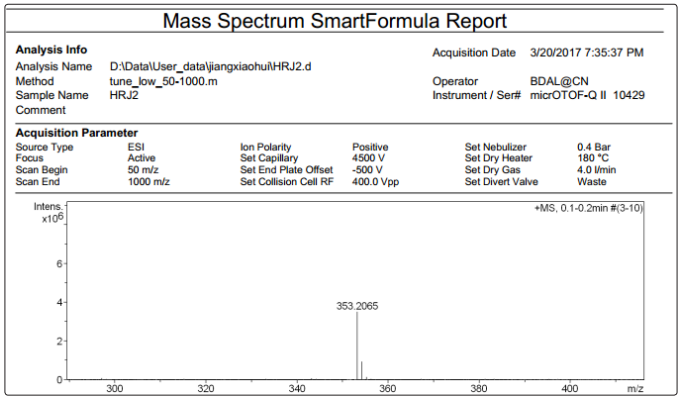

Figure S7: The GC-MS spectrum of BAP-Boc

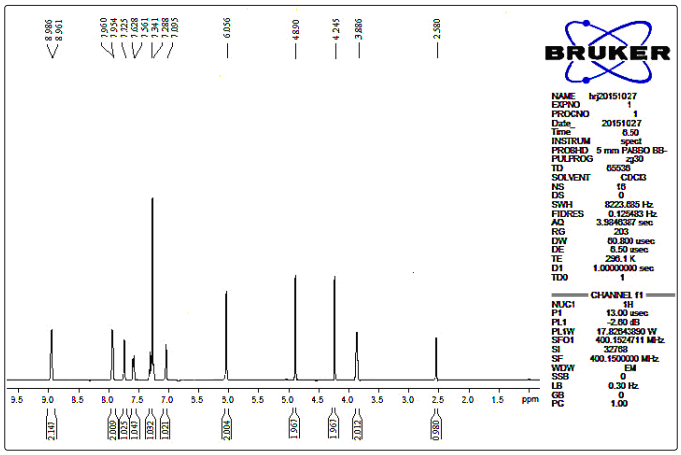

Figure S8: The 1H NMR of BAP

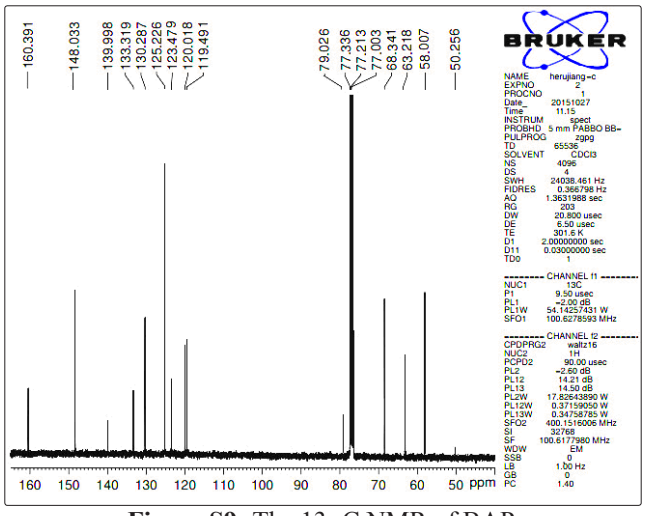

Figure S9: The 13¬C NMR of BAP.

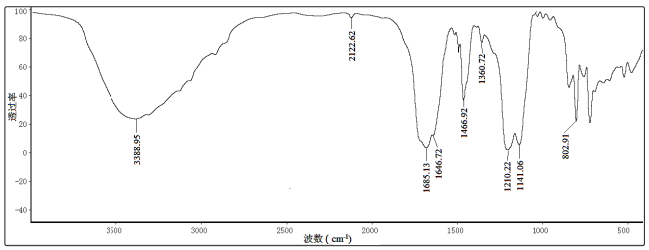

Figure S10: The FT-IR spectrum of BAP.

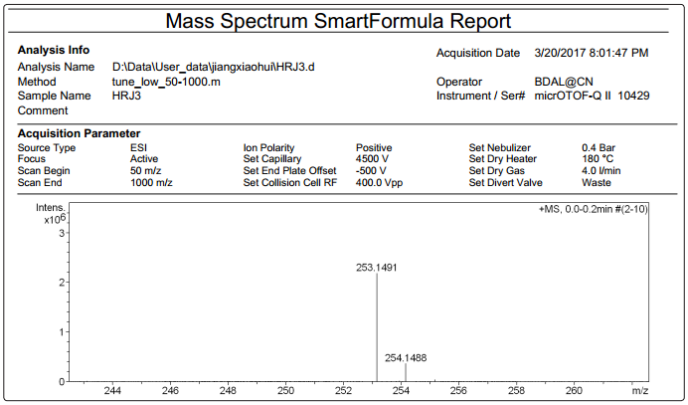

Figure S11: The GC-MS spectrum of BAP.

HYP: ^{1}H NMR (400 MHz, $CDCl_3$, TMS, ppm): δ 8.602-8.589 (d, 2H), δ 7.309-7.282 (t, 2H), δ 4.647 (s, 2H), δ 4.263-4.257 (d, 2H), δ 2.514 (t, 1H); ^{13}C NMR (100 MHz, $CDCl_3$, TMS, ppm): δ 149.730, 146.780, 121.991, 78.977, 69.772, 57.892, 50.727; FT-IR (KBr, cm-1): 3292.43, 3032.03, 2113.22, 1605.26, 1562.56, 1104.60.

BAP-boc: ^{1}H NMR (400 MHz, $CDCl_3$, TMS, ppm): δ 9.420-9.406 (d, 2H), δ 7.954-7.941 (d, 2H), δ 7.749 (s, 1H), δ 7.605-7.586 (d, 1H), δ 7.315 (s, 1H), δ 7.054 (s, 1H), δ 6.160 (s, 2H), δ 4.854 (s, 2H), δ 4.357 (s, 2H), δ 2.557 (s, 1H), δ 1.517 (s, 9H); ^{13}C NMR (100 MHz, $CDCl_3$, TMS, ppm): δ 158.684, 152.805, 144.387, 139.936, 133.306, 130.298, 125.212, 123.482, 120.013, 119.497, 80.767, 78.023, 68.471, 63.632, 58.791, 50.695, 28.301; FT-IR(KBr, cm-1): 3436.04, 3056.07, 3010.29, 2115.40, 1711.94, 1641.66, 1611.43, 1316.48, 1243.55, 1103.39; GC-MS(m/z): 353.2065 M^+.

BAP: ^{1}H NMR (400 MHz, $CDCl_3$, TMS, ppm): δ 8.986-8.961 (d, 2H), δ 7.960-7.954 (d, 2H), δ 7.725 (s, 1H), δ 7.628-7.561 (d, 1H), δ 7.341 (s, 1H), δ 7.095 (s, 1H), δ 6.056 (s, 2H), δ 4.890 (s, 2H), δ 4.245 (s, 2H), δ 3.886 (s, 2H), δ 2.580 (s, 1H) ; ^{13}C NMR (100 MHz, $CDCl_3$, TMS, ppm): δ 160.391, 148.033, 139.998, 133.319, 130.287, 125.226, 123.479, 120.018, 119.491, 79.026, 68.341, 63.218, 58.007, 50.256; FT-IR(KBr, cm-1): 3388.95, 2122.62, 1685.13, 1646.72, 1466.92, 1360.72, 1210.22, 1141.06, 802.91; GC-MS(m/z): 253.1491 M^+.

Weight loss measurement

5 M HCl solution was prepared by diluting the concentrated 37% HCl with tri-distilled water. The concentration range of BAP was set from 0 to 70 ppm.

X70 steel coupons (3 cm × 1.5 cm × 0.2 cm) were abraded with a series of emery papers (grade 240–1600#) until a smooth surface was obtained, degreased with acetone, washed with triply distilled water, and dried by air before tests.

The corrosion parameters obtained by means of weighting loss measurements for X70 steel in the absence and presence of different concentrations of BAP in 5 M HCl at 303-363 K for 24 h of immersion. The experiments were done by triplicate and the average value of the weight loss was used to calculate the corrosion rate (v), the inhibition efficiency (η_w) and surface coverage (Θ) according to the following equations.

$$\upsilon = \frac{W}{St} \quad (9)$$

$$\eta_w = \frac{\upsilon_0 - \upsilon}{\upsilon_0} \times 100\% \quad (10)$$

$$\theta = \frac{\upsilon_0 - \upsilon}{\upsilon_0} \quad (11)$$

Where W is the weight loss of X70 steel, S is the total area of the mild steel sheet, t is the immersion time, v_0 and v are the corrosion rate without and with inhibitor, respectively.

Electrochemical measurements

The electrochemical experiments were performed on CHI760E electrochemical workstation controlled with a computer. The three-electrode electrochemical cell was used with X70 steel as the working electrode, platinum sheet as the auxiliary electrode and Ag/AgCl electrode as the reference electrode. All the potential values reported in this paper are referred to this electrode. The working electrode was prepared in cylindrical rod of X70 steel with an exposure surface of 0.24 cm^2, while the rest of the rod was masked with resin. Prior to each test, the working electrode was abraded with SiC emery paper (240 to 1600 grit), cleaned with ethanol and washed with tri-distilled water, and finally dried at room temperature. The electrode was immersed in test solution for 30 min to attain a stable state before each measurement. All electrochemical tests had been performed in aerated solutions at 30°C.

The Tafel polarization curves were measured by polarizing to ±200 mV with respect to open circuit potential (OCP) at a scan rate of 0.333 mV s^{-1}. Inhibition efficiency was calculated by the corrosion current density values [25]:

$$\eta_p\% = \frac{I^0_{corr} - I_{corr}}{I^0_{corr}} \times 100 \quad (12)$$

Where I^0_{corr} and I_{corr} are the corrosion current density in absence and presence of BAP, respectively.

Electrochemical impedance spectroscopy (EIS) experiments were performed at open potential circuit in the frequency range from 100 kHz to 0.01Hz, with a signal amplitude perturbation of 5 mV. The inhibition efficiency was calculated by the equation as follows:

$$\eta_z\% = \frac{R_c - R^0_c}{R_c} \times 100 \quad (13)$$

Where R^0_{ct} and R_{ct} represent charge transfer resistance values without and with the inhibitor, respectively.

Results and Discussion

The possibility analysis for corrosion inhibition of BAP

Quantum chemical calculations have been identified as worthwhile tools for elucidating the relative reactivity of molecules [26]. Figure 2 depicts the optimized structures, HOMO and LUMO maps of the inhibitor BAP and the two moieties MBA and HYP. It demonstrates amazingly that the pyridinium ring in HYP and benzene ring in MBA contribute mainly to the HOMO and LUMO of the two molecules. However, for BAP, pyridinium ring contributes mainly to LUMO while benzene ring mainly to HOMO, hinting that the aromatic rings perform differently in corrosion inhibition. From the structure characteristic of the two moieties in BAP, we see clearly that the positive charged pyridinium ring is ready for accepting electrons, so, pyridinium ring takes on the character of LUMO. On the other hand, NH_2 group transfers electron to benzene ring via conjugation, making the ring electron abundant. So, benzene ring presents the character of HOMO. Therefore, BAP possesses the ability to donating electron to metal and to accept electron from metal at the same time, inferring a mix-type inhibitor of BAP.

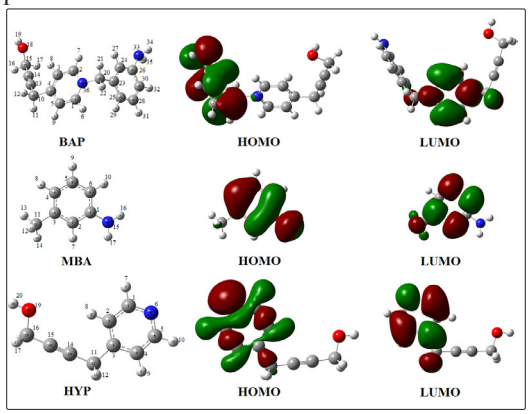

Figure 2: The optimized structure, HOMO, LUMO of the inhibitor molecules using DFT/B3LYP/6-31G (d,p).

Mulliken charge distributions analysis is widely used for the prediction of the adsorption center of inhibitors. The data in Table S1 manifests that the most negative atomic charges happen to the N or O atomic for the three molecules, indicating adsorption centers being N and O atoms [27, 28].

Table S1: Mullikan atomic charges of MBA, HYP and BAP by B3LYP/6-31(d, p) method

MBA		HYP		BAP	
Atom	Mullikan atomic charges	Atom	Mullikan atomic charges	Atom	Mullikan atomic charges
C1	0.2776	C1	0.0848	C1	0.1627
C2	-0.1496	C2	-0.1139	C2	0.1761
C3	0.1210	C3	0.1172	C3	-0.1340
C4	-0.1304	C4	-0.1137	C4	0.1458
C5	-0.0887	C5	0.0877	C5	-0.1356
C6	-0.1182	N6	-0.4318	H6	0.1777
H7	0.0603	H7	0.0997	H7	0.1943
H8	0.0667	H8	0.1173	H8	0.1834
H9	0.0784	H9	0.0815	H9	0.1559
H10	0.0670	H10	0.0959	C10	-0.3446
C11	-0.3809	C11	-0.3412	H11	0.1832
H12	0.1230	H12	0.1500	H12	0.1821
H13	0.1136	H13	0.1490	C13	0.0339
H14	0.1094	C14	0.0669	C14	0.0336
N15	-0.6571	C15	-0.0067	C15	-0.0495
H16	0.2541	C16	-0.0551	H16	0.1358
H17	0.2538	H17	0.1130	H17	0.1358
		H18	0.1130	O18	-0.5345
		O19	-0.5257	H19	0.3268
		H20	0.3118	C20	-0.1399
				H21	0.1733

				H22	0.1626
				C23	0.0565
				C24	-0.1541
				C25	-0.1224
				C26	0.3079
				H27	0.0884
				C28	-0.0877
				H29	0.0902
				C30	-0.1045
				H31	0.1175
				H32	0.1074
				N33	-0.6587
				H34	0.2744
				H35	0.2804
				N36	-0.4199

According to the frontier molecular orbital theory, the formation of a transition state occurs due to interactions between the frontiers orbitals (HOMO and LUMO) of the reactants [29]. Higher values of E_{HOMO} infer the molecule more likely donating electrons to acceptor molecules with a suitable LUMO. In contrast, lower values of E_{LUMO} imply a higher electron accepting ability of the molecule [26]. The ΔE reflects the stability of a molecule, smaller value of ΔE suggests the molecule potentially adsorbing more easily on metal surface, the reactivity of the molecule towards metal surface being enhanced, thus, leading to increased inhibition efficiency of the molecule [30]. The data in Table 2 manifest that BAP with the lowest ΔE value (3.9835 eV) will adsorb onto Fe surface easier than MBA (ΔE =5.1538 eV) and HYP (ΔE =6.2758 eV).

Table 2: The calculated parameters of MBA, HYP and BAP

Species	MBA	HYP	BAP
E_{total}(ev)	-8892.4787	-13010.2819	-21880.9480
E_{HOMO}(eV)	-5.4095	-6.9187	-10.3669
E_{LUMO}(eV)	-0.2557	-0.6428	-6.3834
$\Delta E_{HOMO-LUMO}$ (eV)	5.1538	6.2758	3.9835
Ionization potential I (eV)	5.4095	6.9187	10.3669
Electron affinity A (eV)	0.2557	0.6428	6.3834
Electronegativity χ (eV)	2.8326	3.7808	8.3751
Chemical hardness η (eV)	2.5769	3.1379	1.9917
Chemical softness S $(eV)^{-1}$	0.3881	0.3187	0.5021
Molecular volume V($Å^3$)	163.5005	191.9910	294.6563
Binding energy (kcal/mol)	45.4894	54.4558	65.5826

According to Principle of Maximum Hardness (PMH) [31, 32], chemical hardness can be considered as a measure of stability, and molecules having large chemical hardness values are very stable and not effectively against the corrosion of metals. On the other hand, softness is a measure of polarizability of molecules and soft molecules act as good corrosion inhibitors. In Table 2, the calculated results indicate BAP with the smallest chemical hardness and the largest softness values will be the best inhibitor of the three.

The molecular volume (V) may connect with the surface coverage of metal by inhibitors [33], and it may be proportional to inhibition efficiency, especially at lower concentration of the inhibitor. The data in Table 2 show that the volume of BAP is larger than the volume of MBA and HYP, which indicates that the inhibition performance of BAP is better than that of MBA and HYP.

The adsorption behavior of BAP, BMA and HYP molecule on Fe (100) surface was performed with molecular dynamic simulation the system reaches equilibrium when temperature and energy balance (Figure S12).

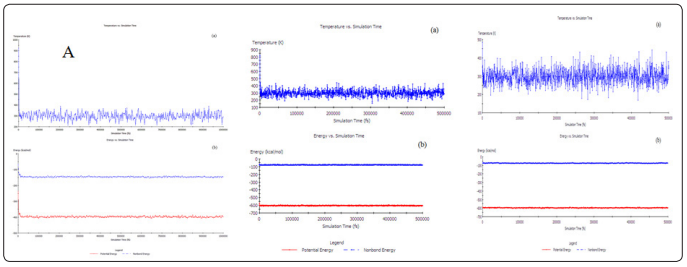

Figure S12: (a) Temperature equilibrium curve and (b) energy fluctuation curves for (A)BAP , (B) MBA and (C) HYP adsorption on Fe (100) surface

Figure 3 shows the snapshot of the top view and side view for the lowest energy configuration of single BAP molecule adsorbing on the Fe (100) surface (those for MBA and HYP in (Figures S13 & S14). By inspection of Figure 3, we could observe that BAP adsorbs close to Fe (100) surface, a chemical interactions can possibly occur through reactive sites in the molecule and on the metal surface. In this case, BAP molecule protects the steel surface from the aggressive medium by adsorbing on the Fe (100) surface in a planar form [34].

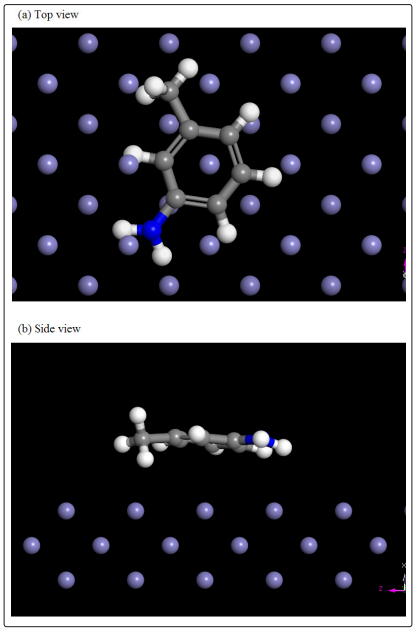

Figure S13: Equilibrium configuration of MBA on Fe (100) surface obtained by molecular dynamic simulation.

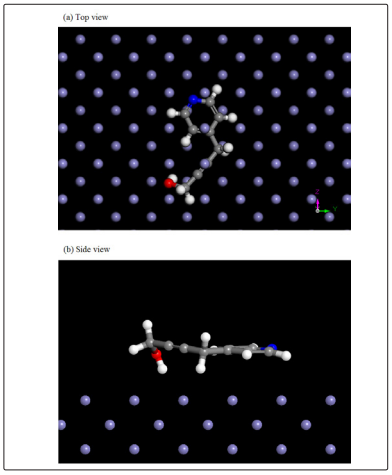

Figure S14: Equilibrium configuration of HYP on Fe (100) surface obtained by molecular

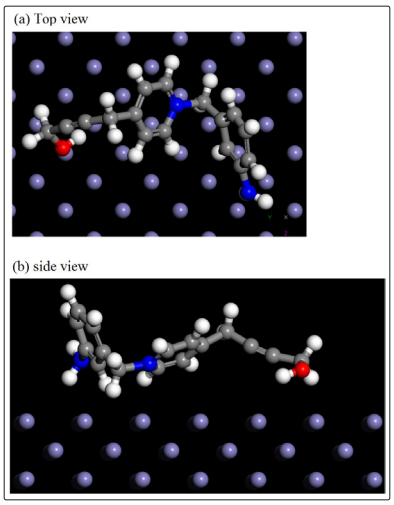

Figure 3: Equilibrium configuration of BAP on Fe (100) surface obtained by molecular dynamic simulation.

The higher value of binding energy suggests easier adsorption of inhibitor on the Fe (100) surface [35]. As can be seen from Table 2, adsorption energy of BAP is larger than those of MBA and HYP, so BAP molecules can easily replace the water molecules adsorbed readily on Fe surface, thereby protecting the X70 steel from corrosion.

In general, all the parameters from theoretical calculation specify that BAP has the lowest value, largest molecular volume and highest binding energy with Fe compared with the two moieties (MBA and HYP), suggesting good corrosion inhibition performance of BAP. Therefore, the chemical combination of MBA with HYP is promising to create an effective inhibitor BAP.

Inhibition performance of BAP on X70 steel surface in HCl solution

Weight loss measurement and data analysis: Figure 4 reveals inhibition efficiency of BAP with different concentrations for X70 steel immersed in 5.0 M HCl at 30-90 °C for 24 h. The inhibition efficiency increases with augmented concentration of BAP and reaches 95.72% at 70 ppm (at 90 °C) (Table S2). It is well recognized that the inhibitor molecules could be directly adsorbed on the mild steel surface through electrostatic interactions between the negatively charged metal surface and the cationic inhibitor molecules. The positively charged inhibitor molecules can also adsorb on cathodic sites of the metal in competition with hydrogen ions [36]. And the adsorption of BAP molecules is faster than that of hydrogen ions. With adding concentration, the coverage of BAP on X70 steel is enlarged, leading to high inhibition efficiency.

Table S2: Weight loss measurement results of X70 steel immersed in 5 M HCl in presence and absence various concentrations of BAP at different temperatures for 24 h (30-90).

Temperature	C (ppm)	W (g)	υ (mg/cm² h)	η(%)
30 °C	0	0.4281	1.8263	/
	10	0.2423	1.0373	43.19
	20	0.1384	0.5948	67.43
	30	0.0905	0.3849	78.92
	40	0.0605	0.2586	85.84
	50	0.0451	0.1922	89.48
	60	0.0404	0.1729	90.53
	70	0.0374	0.1599	91.24
45 °C	0	1.2194	5.2305	/
	10	0.6733	2.8713	45.11
	20	0.3753	1.5962	69.49
	30	0.2294	0.9884	81.10
	40	0.1653	0.7073	86.48
	50	0.1059	0.4598	91.21
	60	0.1052	0.3741	92.85
	70	0.0807	0.3468	93.37
60 °C	0	2.8301	12.5035	/
	10	1.5406	6.6336	46.94
	20	0.8064	3.4903	72.08
	30	0.4586	1.9762	84.19
	40	0.3632	1.5560	87.55
	50	0.2104	0.9138	92.69
	60	0.1874	0.8023	93.58
	70	0.1580	0.6866	94.50
75 °C	0	4.3890	20.1453	/
	10	2.2524	9.9869	50.42
	20	1.2175	5.2320	74.03
	30	0.6695	2.9617	85.30
	40	0.4911	2.1174	89.49
	50	0.2956	1.2911	93.59
	60	0.2574	1.1298	94.39
	70	0.2225	0.9711	95.18
90 °C	0	7.1603	31.1770	/
	10	3.5023	14.9694	51.97
	20	1.6707	7.3991	76.26
	30	0.9214	4.0468	87.02
	40	0.6485	2.7777	91.09
	50	0.4055	1.7639	94.34
	60	0.3435	1.4872	95.23
	70	0.3109	1.3354	95.72

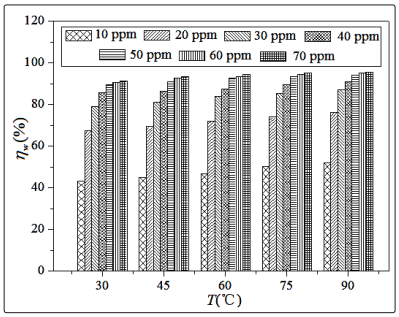

Figure 4: Inhibition efficiency of BAP for X70 steel immersed in 5 M HCl solution for 24 h at different temperatures.

The corrosion inhibition efficiency of organics on the mild steel surface has been found to decrease with increasing temperature [37]. However, BAP functions differently from general corrosion inhibitors do. The inhibition efficiency of BAP increases with raising temperature. The data in Table S1 display that the inhibition efficiency increase from 67.43% to76.26% as the temperature is elevated from 30 to 90 °C (at 20 ppm of BAP).

Theoretic calculation elucidates that LUMO of BAP focuses on pyridinium ring and HOMO of BAP on benzene ring. So, the two aromatic rings performing differently on X70 steel: benzene ring denoting electrons to X70 steel, at the same time, pyridinium ring accepting electron from the metal. In such a way, BAP molecules are preferentially and firmly adsorbed on the surface of X70 steel. The transfer and share of electrons between BAP molecules and iron atoms are facilitated by elevating temperature, and the chemical adsorption of BAP becomes more evident on X70 steel surface with augmented temperature, which in turn enhances the corrosion inhibition efficiency of the BAP at higher temperature [38].

Adsorption behavior of an inhibitor on a metal surface can be explained by fitting the experimental data into suitable adsorption isotherm. Several isotherms including Frumkin, Langmuir, Temkin, Freundlich, Bockris–Swinkels and Flory–Huggins isotherms were applied to fit the experimental data. It is found that the adsorption of BAP on X70 steel surface obeys Langmuir adsorption isotherm [39]:

$$\frac{c}{\theta} = \frac{1}{K} + c \qquad (14)$$

Where Θ is the fractional surface coverage, c is the inhibitor concentration and K is the equilibrium constant of the adsorption process. The linear relationship of c/θ versus c, depicted in Figure 5, suggests that the adsorption of BAP on the mild steel obeys Langmuir adsorption isotherm. This model assumes that the solid surface contains a fixed number of adsorption sites and each site holds one adsorbed species [40].

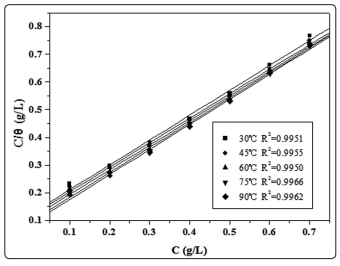

Figure 5: Langmuir isotherm plots for the adsorption of BAP on X70 steel surface.

K_{adas} values were used to calculate the standard free energy of the adsorption (ΔG^0_{ads}) of BAP molecules according to the following equation [41]:

$$\Delta G^0_{ads} = -RT\ln(55.5K_{ads}) \qquad (15)$$

Where 55.5 is the mole concentration of water, R is the gas constant (8.314 J mol^{-1} K^{-1}) and T is the absolute temperature (K). The calculated K_{ads} and ΔG^0_{ads} values of BAP are reported in Table 3. In physical adsorption, ΔG^0_{ads} value is -20 kJ mol^{-1} or more positive, suggesting an electrostatic interaction between inhibitor molecules and metal surface. In chemisorption, the value is close to -40 kJ mol^{-1}, indicating charge share and transfer between the organic molecules and the metal surface to form a coordinate bond [42]. The calculated value of ΔG^0_{ads} in this study is between -20 and -40 kJ mol^{-1}, elaborating that BAP adsorbs on X70 steel surface via both physisorption and chemisorption [43, 44].

Table 3: Thermodynamic parameters of BAP adsorption on X70 steel

inhibitor	T(K)	n	R^2	Intercept (g/L)	k_{ads} (L/g)	ΔG^0_{ads} (kJ mol^{-1})	ΔH^0_{ads} (kJ mol^{-1})	ΔS^0_{ads} (J mol^{-1})
BAP	303.15	0.8851	0.9951	0.0124	80.5135	-28.47		113.77
	318.15	0.8854	0.9955	0.0115	86.7303	-30.08		94.53
	333.15	0.8905	0.9950	0.0105	95.6938	-31.77	6.02	95.35
	348.15	0.9018	0.9966	0.0093	108.1081	-33.55		96.37
	363.15	0.9063	0.9962	0.0085	118.3432	-35.27		97.12

The standard enthalpy of adsorption (ΔH^0_{ads}) can be obtained according to Gibbs–Helmholtz equation:

$$\left[\frac{\partial\left(\Delta G^0_{ads}/T\right)}{\partial T}\right]_p = \frac{-\Delta H^0_{ads}}{T^2} \qquad (16)$$

The following expression can be deduced through the integration of the partial derivative Eq. (16):

$$\frac{\Delta G^0_{ads}}{T} = \frac{\Delta H^0_{ads}}{T} + k \qquad (17)$$

Thus, $\Delta H^0_{ads}/T$ decreases with $1/T$ in a linear mode (Figure 6). Then, ΔH^0_{ads} is got from the slope of the line, and the positive value suggests an endothermal adsorption process.

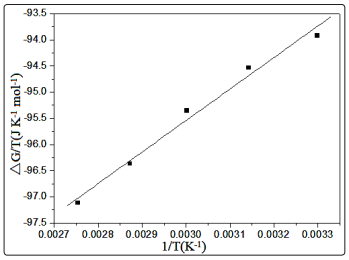

Figure 6 : Plots of /T versus 1/T.

The standard adsorption entropy (ΔS^0_{ads}) can be acquired by the thermodynamic basic equation:

$$\Delta S^0_{ads} = \frac{\Delta H^0_{ads} - \Delta G^0_{ads}}{T} \qquad (18)$$

The ΔS^0_{ads} values in the presence of BAP are tabulated in Table 3. As we know, X70 steel surface is covered with water before the adsorption of BAP molecules. Then the adsorbed water molecules are replaced by BAP which is a surfactant by nature and prefers adsorbing on X70 steel surface to staying in aqueous phase owing to the repelling force of water molecules in bulk solution. With the replacement of water by BAP on X70 steel surface, the entropy of BAP molecules reduces while that of water molecules increases due to the restoration of their freedom. Therefore, it is plausible that the entropy change in the whole process of BAP adsorption and water desorption is positive.

Kinetic model can be used to explore the effect of BAP on the kinetics of X70 steel corrosion. The apparent activation energy (E_a) for X70 steel corrosion in acid and in inhibited acid solution was determined from Arrhenius equation as follows:

$$\ln \upsilon = -\frac{E_a}{RT} + \ln A \qquad (19)$$

Where υ is the corrosion rate, E_a the apparent activation energy, A the pre-exponential factor, T and R have the same meaning as those in Equation (15). Figure 7 illustrates the Arrhenius plots of ln υ against 1/T in the presence and absence of BAP at different temperature. The values of E_a and A, obtained from the slopes and intercepts of the Arrhenius plots, respectively, are tabulated in Table 4. Studies report that the value of E_a for inhibited solution higher than that for uninhibited solution can be interpreted as physical adsorption, while the value of E_a for inhibited solution lower than that for uninhibited solution is considered as chemical adsorption [45]. In the presence of BAP, the value of E_a is lower than that in uninhibited solution, which further confirms that the adsorption of the BAP on the surface of the X70 steel sheet is typical chemical adsorption.

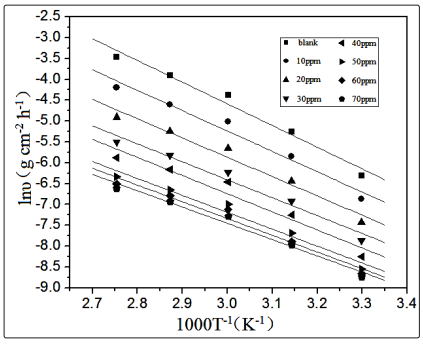

Figure 7: Plots of versus 1/T.

Table 4: Activation parameters for X70 steel dissolution in 5 M HCl with different concentrations of BAP at 30–90 °C

C (ppm)	Ea (kJ mol^{-1})	A (g cm^{-2} h^{-1})	R^2
0	43.23	66138.08	0.9725
10	40.57	12077.51	0.9653
20	38.40	2936.87	0.9611
30	35.78	666.67	0.9614
40	34.15	543.65	0.9522
50	33.74	144.21	0.9602
60	33.34	108.77	0.9607
70	32.48	71.07	0.9706

The activation enthalpy $\Delta H^{\#}$ and activation entropy $\Delta S^{\#}$ can be obtained from the transition state equation:

$$\upsilon = \left(\frac{RT}{Nh}\right)\exp\left(\frac{\Delta S^{\neq}}{R}\right)\exp\left(\frac{-\Delta H^{\neq}}{RT}\right) \qquad (20)$$

Where N is the Avogadro's number, h the Planck's constant, T and R have the same meaning as those in Equation (15). Plotting ln (υ/T) against 1/T yields straight lines (Figure 7). The activation enthalpy $\Delta H^{\#}$ and activation entropy$\Delta S^{\#}$can be obtained from the slop and intercept of the linear plots, respectively, and the data obtained are given in Table 5. The positive sign of enthalpy reflects the endothermic nature of steel dissolution process, meaning that dissolution of steel is difficult [46]. $\Delta S^{\#}$ In the presence of the inhibitor is negative, suggesting that an increase in ordering takes place in going from reactant to the activated complex.

Table 5: Activation parameters for X70 steel dissolution in 5 M HCl in the presence and absence of various concentrations of BAP at different temperatures

C (ppm)	$\Delta H^{\#}$ (kJ mol-1)	($\Delta S^{\#}$ mol^{-1} K^{-1})	R^2
0	40.48	-162.57	0.9681
10	37.82	-175.97	0.9593
20	35.65	-187.72	0.9541
30	33.03	-200.05	0.9538
40	32.39	-205.74	0.9460
50	30.95	-212.78	0.9520
60	30.58	-215.12	0.9524
70	29.72	-218.66	0.9639

Tafel polarization measurement

Tafel polarization studies were carried in order to understand the process of anodic oxidative metallic dissolution and cathodic reductive hydrogen evolution. The Tafel polarization curves for X70 steel electrode in 5 M HCl in the absence and presence of different concentration of BAP are illustrated in Figure 8, and the figure manifests that both cathodic and anodic Tafel curves of X70 steel in absence and presence of BAP are almost parallel, suggesting that the addition of BAP in the aggressive solution does not change the mechanism of metal dissolution and the hydrogen evolution reaction. The corresponding electrochemical parameters are listed in Table 6, such as corrosion potential (E_{corr}), cathodic (β_c) and anodic (β_a) slopes, and corrosion current density (I_{corr}) obtained by the extrapolation of Tafel lines. It is clear that presence of BAP significantly reduces corrosion current densities for both anodic and cathodic half reactions. For example, the current density diminishes from 404 to 62.2 μA cm^{-2} when the concentration of BAP rises from 10 to 60 ppm, and the inhibition efficiency increases accordingly from 48.78 to 92.12%. An inhibitor can be defined as cathodic or anodic or mix type inhibitor according to ΔE_{corr}. In the presence of BAP, the shifts of corrosion potential is about 14 mV (vs. Ag/AgCl), indicating that the BAP is of mix-type inhibitor.

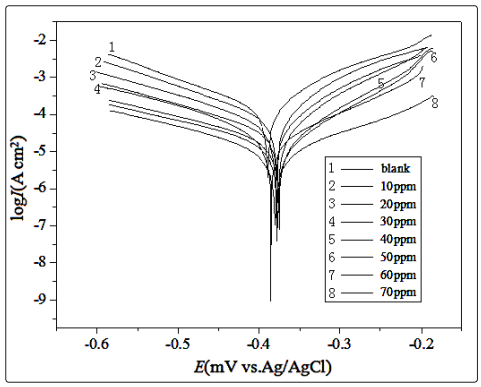

Figure 8: Tafel polarization curves of X70 steel in the absence and presence of BAP in 5 M HCl at 30 °C

Table 6: Tafel polarization parameters of X70 steel in different concentration of BAP in 5 M HCl at 30 °C.

inhibitor	C (ppm)	E_{corr} (mV)	I_{corr} (mA cm^{-2})	β_a (V/dec)	$-\beta_c$ (V/dec)	R_p (Ω)	η_p%
blank	0	-389.0	0.789	0.109	0.132	137.0	/
	10	-378.2	0.404	0.096	0.131	248.3	48.78
	20	-379.0	0.225	0.090	0.140	433.2	71.44
	30	-376.1	0.157	0.086	0.151	632.5	80.09
BAP	40	-378.4	0.104	0.107	0.139	1058.3	86.90
	50	-375.1	0.076	0.081	0.175	1318.5	90.40
	60	-377.1	0.062	0.082	0.181	1628.8	92.12
	70	-382.0	0.048	0.142	0.164	2826.3	93.90

Electrochemical impedance spectroscopy

The corrosion inhibition of BAP on X70 steel was also examined by electrochemical impedance spectroscopy. The Nyquist diagrams of X70 steel (Figure 9) demonstrates enlarged radius of the impedance when the BAP is added to the corrosive solution, hinting an improved resistance against acid corrosion [47]. The capacitive loop is related to the charge transfer process of the metal corrosion and double layer behavior. The depressed semi-circle in Nyquist curves is generally attributed to the frequency dispersion as well as inhomogeneity or roughness of metal surface [48].

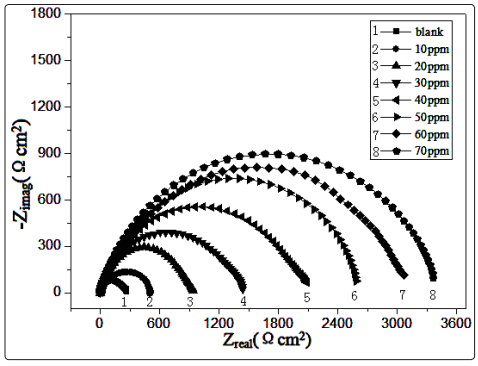

Figure 9: Nyquist plots of X70 steel in the absence and presence of BAP in 5 M HCl at 30 °C.

The Bode and phase angle plots for mild steel in 5 M HCl with and without BAP are plotted in Figure 10. The increase of impedance at low frequencies in Bode plots confirms the enhanced protection with augmented concentration of BAP. According to the appearance of phase angle plots, increasing the concentration of BAP results in more negative values of phase angle, indicating superior inhibition behavior due to more BAP molecule adsorbing on metal surface [49].

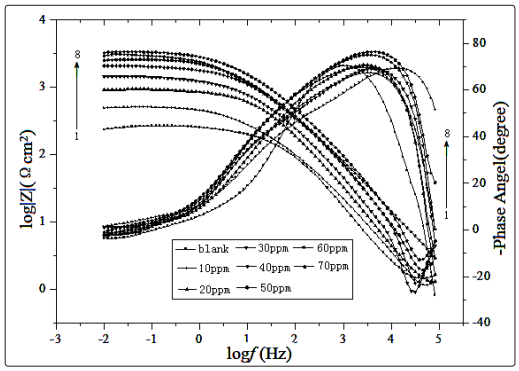

Figure 10: Bode plots of X70 steel without and with different concentrations of BAP.

In order to better interpret EIS results, the equivalent circuit model containing solution resistance (R_s), charge transfer resistance (R_{ct}), film/electrolyte interface resistance (R_2), constant phase element CPE(Q) and double layer capacitance (C_{dl}) is used to fit the experimental results. The impedance function of CPE is represented by the expression [50]:

$$Z_{CPE} = Y_0^{-1}(j\omega)^{-n} \quad (21)$$

Where Y_0 is a proportional factor, ω is the angular frequency, j is imaginary unit. n has the meaning of a phase shift, for n=0, Q represents a resistance; for n=1, a capacitance; for n=0.5, a Warburg element; and for n=1, an inductance. The double layer capacitance (C_{dl}) can be expressed as:

$$C_{dl} = Y_0(\omega''_m)^{n-1} \quad (22)$$

Where ω''_m is the angular frequency at the maximum value of the imaginary part of the impedance spectrum.

The equivalent circuit for data fitting and the measured and fitted curves are shown in (Figure S15). The measured spectra match well to the simulated spectra by the selected equivalent circuit. The fitted impedance parameters of X70 steel are arranged in [Table 7].

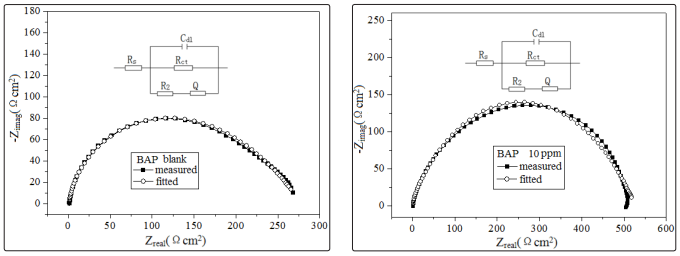

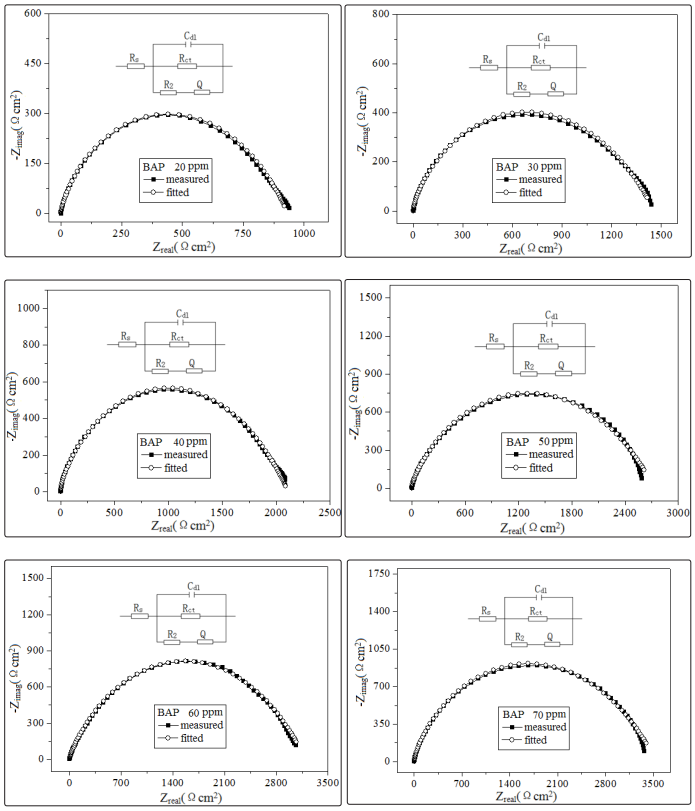

Figure S15: The equivalent electric used for fitting impedance spectra of X70 steel and comparison of experimental EIS data (quadrangle) and simulated (circle).

Table 7: EIS parameters of X70 steel in different concentrations of BAP in 5.0 M HCl at 30 °C

Inhibitor	C (ppm)	R_s (Ω cm²)	C_{dl} (uFcm⁻²)	R_{ct} (Ωcm²)	Q Y_0(uFcm⁻²)	n	R_2 (Ωcm²)	η_Z%
blank	0	1.591	191.8	277	8.18	0.5194	25.34	/
	10	1.380	170.6	526	5.31	0.5863	27.44	47.26
	20	1.409	60.9	932	3.95	0.6339	50.38	70.33
	30	2.492	48.7	1457	2.90	0.5804	85.56	80.96
BAP	40	2.573	44.2	2111	1.77	0.5742	128.70	86.58
	50	1.719	41.3	2712	1.80	0.5962	101.60	89.77
	60	2.632	39.7	3194	9.14	0.5804	15.62	91.31
	70	2.196	37.6	3535	9.42	0.5662	1.975	92.15

The data In Table 7 illustrate a clear trend of elevating polarization resistance accompanied with rapid decline in the double layer capacitance upon increasing concentrations of BAP, which suggests the effective adsorption of large variety of BAP molecules on X70 steel surface. The decreased C_{dl} values with BAP concentration may be due to a decrease in dielectric constant, hence an increased adsorption ability of BAP results in the enhanced protection for X70 steel against dissolution by HCl [47].

The verification of the theoretical calculation results

The inhibition properties of HYB and MAP on X70 steel in 5 M HCl were evaluated by weight loss measurement. The experimental data obtained are listed in Table S3 and in Figure 11. The bars in Figure11 demonstrate that the inhibition performance of MBA is the poorest among the three inhibitors. Elevating the temperature from 30 to 60 °C increases a little the inhibition efficiency of the inhibitors, which may be due to the augmented solubility and the rate of diffusion and adsorption of the inhibitors at higher temperature. However, a further elevated temperature impairs badly the inhibition ability of MBA and HYP, and the inhibition efficiency drops from 12.83% to 4.07% for MAB and from 38.52% to 7.65% for HYP when the temperature is raised from 60 to 90 °C. Amazingly, the inhibition efficiency of BAP keeps rising with elevated temperature even at a concentration as low as 4 μM, which manifests that the inhibition capacity of BAP will be consolidated by high temperature. Comparatively, although the concentration of BAP is only tenth of that for MAB and HYP, the inhibition efficiency of BAP is about 10 times of that for MAB and 8 times of that for HYP. This outcome supports very well the theoretical calculation result. Once again, synergic effect in a molecule may make the molecule of higher inhibition capacity, and it could be applied on the design of new efficient inhibitor.

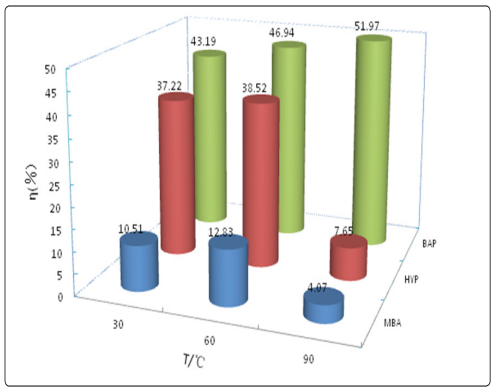

Figure 11: The inhibition efficiency of BAP (10 μM), MBA (40 μM) and HYP (40 μM) by weight loss (5 M HCl, 30, 60, 90 °C).

Conclusion

BAP is a new effective inhibitor. Its inhibition efficiency for X70 steel in 5 M HCl solution is reinforced with increasing temperature. BAP can mitigate the corrosion of X70 steel by deterring corrosion reaction at both anode and cathode. BAP can improve the charge transfer resistance of X70 steel in acid solution. The adsorption of BAP obeys Langmuir adsorption isotherm and is an endothermic and entropy gaining process. BAP can be considered as chemical combination of two moieties, HYP and MBA. And the chemical connection of HYP and MBA not only endow BAP much better inhibitory efficacy against acid corrosion of steel, but also offer BAP the capability of in situ polymerizing on X70 steel surface to form double protective layers, which may demonstrate even stronger resistance against acid corrosion. This work is under way in our laboratory.

Acknowledgements

The authors are very grateful for financial supports from the National Natural Science Foundation of China (21176201).

References

1. Saravanamoorthy S, Velmathi S (2013) Physiochemical interactions of chiral Schiff bases on high carbon steel surface. Corrosion inhibition in acidic media. Prog Org Coat 76: 1527-1535.
2. Bobina M, Kellenberger A, Millet JP, Muntean C, Vaszilcsin N (2013) Corrosion resistance of carbon steel in weak acid

solutions in the presence of L-histidine as corrosion inhibitor. Corros Sci 69: 389-395.

3. Mallaiya K, Subramaniam R, Srikandan SS, Gowri S, Rajasekaran N, et al. (2011) Electrochemical characterization of the protective film formed by the unsymmetrical Schiff's base on the mild steel surface in acid media. Electrochim Acta 56: 3857-3863.
4. Amin MA, Khaled K, Mohsen Q, Arida H (2010) A study of the inhibition of iron corrosion in HCl solutions by some amino acids. Corros Sci 52: 1684-1695.
5. Solmaz R, Altunbas E, Kardas G (2011) Adsorption and corrosion inhibition effect of 2-((5-mercapto-1, 3, 4-thiadiazol-2-ylimino) methyl) phenol Schiff base on mild steel. Mater Chem Phys 125: 796-801.
6. Pournazari S, Moayed MH, Rahimizadeh M (2013) In situ inhibitor synthesis from admixture of benzaldehyde and benzene-1,2-diamine along with $FeCl_3$ catalyst as a new corrosion inhibitor for mild steel in 0.5 M sulphuric acid. Corros Sci 71: 20-31.
7. Moretti G, Guidi F, Fabris F (2013) Corrosion inhibition of the mild steel in 0.5 M HCl by 2-butyl-hexahydropyrrolo [1,2-b] [1,2] oxazole. Corros Sci 76: 206-218.
8. El Adnani Z, Mcharfi M, Sfaira M, Benzakour M, Benjelloun AT, et al. (2013) DFT theoretical study of 7-R-3-methylquinoxalin-2(1H)-thiones (R = H; CH3;Cl) as corrosion inhibitors in hydrochloric acid. Corros Sci 68: 223-230.
9. Tang YM, Zhang F, Hu SX, Cao ZY., Wu ZL, et al. (2013) Novel benzimidazole derivatives as corrosion inhibitors of mild steel in the acidic media. Part I: gravimetric, electrochemical, SEM and XPS studies. Corros Sci 74: 271-282.
10. Kıcıra N, Tansuğ G, Erbil M, Tüken T (2016) Investigation of ammonium (2, 4-dimethylphenyl)-dithiocarbamate asa new, effective corrosion inhibitor for mild steel. Corros Sci 105: 88-99.
11. Hejazi S, Mohajernia S, Moayed MH, Davoodi A, Rahimizadeh M, et al. (2015) Electrochemical quantum chemical study of Thiazolo-pyrimidine derivatives as corrosion inhibitors on mild steel in 1 M H_2SO_4. J Ind Eng Chem 25: 112-121.
12. Yüce AO, Mert BD, Kardaş G, Yazıcı B (2014) Electrochemical and quantum chemical studies of 2-amino-4-methyl-thiazole as corrosion inhibitor for mild steel in HCl solution. Corros Sci 83: 310-316.
13. Döner A, Kardas G (2011) N-Aminorhodanine as an effective corrosion inhibitor for mild steel in 0.5 M H_2SO_4. Corros Sci 53: 4223-4232.
14. Mert BD, Mert ME, Kardas G, Yazıcı B (2011) Experimental and theoretical investigation of 3-amino-1,2,4-triazole-5-thiol as a corrosion inhibitor for carbon steel in HCl medium. Corros Sci 53: 4265-4272.
15. Dutta A, Saha SK, Adhikari U, Banerjee P, Sukul D (2017) Effect of substitution on corrosion inhibition properties of 2-(substitutedphenyl) benzimidazole derivatives on mild steel in 1 M HCl solution: A combined experimental and theoretical approach. Corros Sci 123: 256-266.
16. Mendonça GLF, Costa SN, Freire VN, Casciano PNS, Correia AN, et al. (2017) Understanding the corrosion inhibition of carbon steel and copper in sulphuric acid medium by amino acids using electrochemicaltechniques allied to molecular modelling methods. Corros Sci 115: 41-55.
17. Yıldız R (2015) An electrochemical and theoretical evaluation of 4, 6-diamino-2-pyrimidinethiol as a corrosion inhibitor for mild steel in HCl solutions. Corros Sci 90: 544-553.
18. Dasami PM, Parameswari K, Chitra S (2015) Corrosion inhibition of mild steel in $1MH_2SO_4$ by thiadiazole Schiff bases. Measurement 69: 195-201.
19. Finšgar M, Jackson J (2014) Application of corrosion inhibitors for steels in acidic media for the oil and gas industry: A review. Corros Sci 86: 17-41.
20. Gonçalves RS, Azambuja DS, Lucho AMS (2002) Electrochemical studies of propargyl alcohol as corrosion inhibitor for nickel, copper, and copper/nickel (55/45) alloy. Corros Sci 44: 467-479.
21. Verma C, Quraishi MA, Ebenso EE, Obot IB, Assyry AE (2016) 3-Amino alkylated indoles as corrosion inhibitors for mild steel in 1M HCl: Experimental and theoretical studies. J Mol Liq 219: 647-660.
22. Saha SK, Murmu M, Murmu NC, Banerjee P (2016) Evaluating electronic structure of quinazolinone and pyrimidinone molecules for its corrosion inhibition effectiveness on target specific mild steel in the acidic medium: A combined DFT and MD simulation study. J Mol Liq 224: 629-638.
23. Saha SK, Ghosh P, Hens A, Murmu NC, Banerjee P (2015) Density functional theory and molecular dynamics simulation study on corrosion inhibition performance of mild steel by mercapto-quinoline Schiff base corrosion inhibitor. Physica E 66: 332-341.
24. Gu TB, Chen ZJ, Jiang XH, Zhou LM, Liao YW, et al. (2015) Synthesis and inhibition of N-alkyl-2-(4-hydroxybut-2-ynyl) pyridinium bromide for mild steel in acid solution: Box–Behnken design optimization and mechanism probe. Corros Sci 90: 118-132.
25. Amin MA, Khaled KF, Fadl-Allah SA (2010) Testing validity of the Tafel extrapolation method for monitoring corrosion of cold rolled steel in HCl solutions-Experimental and theoretical studies. Corros Sci 52: 140-151.
26. Bedaira MA, El-Sabbah MMB, Fouda AS, Elaryian HM (2017) Synthesis, electrochemical and quantum chemical studies of some prepared surfactants based on azodye and Schiff base as corrosion inhibitors for steel in acid medium. Corros Sci 128: 54-72.
27. Obi-Egbedi N, Obot IB, El-Khaiary MI (2011) Quantum chemical investigation and statistical analysis of the relationship between corrosion inhibition efficiency and molecular structure of xanthene and its derivatives on mild steel in sulphuric acid. J Mol Struct 1002: 86-96.
28. Hu J, Wang Y, Yu L, Zou Y, Wang Y (2015) An Investigation of a Combined Thiourea and Hexamethylenetetramine as Inhibitors for Corrosion of N80 in 15% HCl Solution: Electrochemical Experiments and Quantum Chemical Calculation. Int J Corros 2015: 1-12.
29. Finsgar M, Lesar A, Kokalj A, Milosev I (2008) A comparative electrochemical and quantum chemical calculation study of BTAH and BTAOH as copper corrosion inhibitors in near neutral chloride solution. Electrochim Acta 53: 8287-8297.
30. Mourya P, Singh P, Tewari AK, Rastogi RB, Singh MM (2015) Relationship between structure and inhibition behaviour of quinolinium salts for mild steel corrosion: experimental and theoretical approach. Corros Sci 95: 71-87.
31. Kaya S, Kaya C (2015) A new method for calculation of molecular hardness: a theoretical Study. Comput Theor Chem

1060: 66-70.
32. Parr RG, Chattaraj PK (1991) Principle of maximum hardness. J Am Chem Soc 113: 1854-1855.
33. Ebenso EE, Kabanda MM, Murulana LC, Singh AK, Shukla SK (2012) Electrochemical and Quantum Chemical Investigation of Some Azine and Thiazine Dyes as Potential Corrosion Inhibitors for Mild Steel in Hydrochloric Acid Solution. Ind Eng Chem Res 51: 12940-12958.
34. Zhang Z, Tian NC, Huang XD, Shang W, Wu L (2016) Synergistic inhibition of carbon steel corrosion in 0.5 M HCl solution by indigo carmine and some cationic organic compounds: experimental and theoretical studies. RSC Adv 6: 22250-22268.
35. Gopiraman M, Selvakumaran N, Kesavan D, Kim I S, Karvembu R (2012) Chemical and Physical Interactions of 1-Benzoyl-3,3-Disubstituted Thiourea Derivatives on Mild Steel Surface: Corrosion Inhibition in Acidic Media. Ind Eng Chem Res 51: 7910-7922.
36. Obot IB, Obi-Egbedi NO, Umoren SA (2009) The synergistic inhibitive effect and some quantum chemical parameters of 2, 3-diaminonaphthalene and iodide ions on the hydrochloric acid corrosion of aluminium. Corros Sci 51: 276-282.
37. Doner A, Solmaz R, Özcan M, Kardas G (2011) Experimental and theoretical studies of thiazoles as corrosion inhibitors for mild steel in sulphuric acid solution. Corros Sci 53: 2902-2913.
38. Ahamad I, Quraishi MA (2009) Bis (benzimidazol-2-yl) disulphide: an efficient water soluble inhibitor for corrosion of mild steel in acid media. Corros Sci 51: 2006-2013.
39. Liao LL, Mo S, Luo HQ, Feng YJ, Yin HY, et al. (2017) Relationship between inhibition performance of melamine derivatives and molecular structure for mild steel in acid solution. Corros Sci 124: 167-177.
40. Ali SA, Saeed G.T, Rahman US (2003) The isoxazolidines: a new class of corrosion inhibitors of mild steel in acidic medium. Corros Sci 45: 253-266.
41. Kıcır N, Tansuğ G, Erbil M, Tüken T (2016) Investigation of ammonium (2, 4-dimethylphenyl)-dithiocarbamate as a new, effective corrosion inhibitor for mild steel. Corros Sci 105: 88-99.
42. Pavithra MK, Venkatesha TV, Punith Kumar M.K, Tondan HC (2012) Inhibition of mild steel corrosion by Rabeprazole sulfide. Corros Sci 60: 104-111.
43. Soltani N, Salavati H, Rasouli N, Paziresh M, Moghadasi (2016) A Adsorption and corrosion inhibition effect of schiff base ligands on low carbon steel corrosion in hydrochloric acid solution. Chem Eng Commun 203: 840-854.
44. Singh P, Quraishi MA (2016) Corrosion inhibition of mild steel using novel bis Schiff's bases as corrosion inhibitor: electrochemical and Surface measurement. Meas 86: 114-124.
45. Sĭgırcık G, Yildirim D, Tüken T (2017) Synthesis and inhibitory effect of N,N'-bis(1-phenylethanol)ethylenediamine against steel corrosion in HCl Media. Corros Sci 120: 184-193.
46. Mu GN, Li XM, Li F (2004) Synergistic inhibition between o-phenanthroline and chloride ion on cold rolled steel corrosion in phosphoric acid. Mater Chem Phys 86: 59-68.
47. Azzaoui K, Mejdoubi E, Jodeh S, Lamhamdi A, Rodriguez-Castellón E, et al. (2017) Eco friendly green inhibitor Gum Arabic (GA) for the corrosion control of mild steel in hydrochloric acid medium. Corros Sci 129: 70-81
48. 48. Yadav M, Behera D, Kumar S, Sinha RR (2013) Experimental and Quantum Chemical Studies on the Corrosion Inhibition Performance of Benzimidazole Derivatives for Mild Steel in HCl. Ind Eng Chem Res 52: 6318-6328.
49. Mahdavian M, Ashhari S (2010) Corrosion inhibition performance of 2-mercaptobenzimidazole and 2-mercaptobenzoxazole compounds for protection of mild steel in hydrochloric acid solution. Electrochim Acta 55: 1720-1724.
50. Zhang F, Tang YM, Cao ZY, Jing WH, Wu ZL, et al. (2012) Performance and theoretical study on corrosion inhibition of 2-(4-pyridyl)-benzimidazole for mild steel in hydrochloric acid. Corros Sci 61: 1-9.